PCCP

Accepted Manuscript

ROYAL SOCIETY OF CHEMISTRY

www.rsc.org/pccp

Half-metallic and magnetic properties in nonmagnetic element embedded graphitic carbon nitride sheets

Bo Meng [a], Wen-Zhi Xiao [b]*, Ling-ling Wang [c]*, Li Yue [a], Song Zhang [a], Hong-yun Zhang [a]

[a] College of Physics and Electronic Engineering, Kaili University, Kaili 556011, China

[b] Department of Physics and Mathematics, Hunan Institute of Engineering, Xiangtan 411104, China

[c] School of Physics and Electronics, Hunan University, Changsha 410082, China

Abstract: We have investigated the structures, electronic structure and magnetic properties of the triazine-based g-C_3N_4 (gt-C_3N_4) monolayer doped with B, Al, and Cu atoms based on density functional theory using *ab* initio calculations. B atom prefers to be situated at the center of triazine ring, whereas Al and Cu atoms tend to locate above the center of triazine ring. The doping at interstitial sites results in nonplanar structures which are thermodynamically stable. Each dopant atom induces a total magnetic moment of 1.0 μ_B which mainly arises from the p_z orbitals because the *n*-type doping injects unpaired electrons into anti-π orbitals. The results obtained from GGA-PBE and HSE06 schemes show that all the doped systems exhibit half-metallic behaviors. B- and Al-doped systems are ferromagnetic ground state, while Cu-doped case is anti-ferromagnetic ground state. The long-range half-metallic ferromagnetic order is attributed to the *p-p* interactions. In particular, the estimated Curie temperature implies that the systems doped with B and are potential candidates for spintronics applications in future.

Keywords: Half-metallicity; Magnetic property; gt-C_3N_4; Density functional theory

*Corresponding author:
E- mail: xiaowenzhi@hnu.edu.cn; llwang@hnu.edu.cn
Tel: +86 0732 58680254； Fax: +86 0732 58683562

1. Introduction

In the field of spintronics, a new generation of electronic devices, so-called spintronic devices, that can simultaneously process and store information by controlling and manipulating both the charge and spin degrees of freedom of carriers.[1] Considerable research activities have been devoted to search for half metallic materials that can generate 100% spin-polarized currents at the Fermi level, making them suitable for the spintronic devices.[2, 3] Motivated by the miniature trend in conventional semiconductor industry, scientists have begun to turn their attention to designing and developing low dimensional candidates for electrionic devices of the next generation. Monolayer materials have the particular dimensionality, compared with their bulk counterparts, and hence exhibit different properties, such as electricity, optics, magnetism and mechanics. It was believed that the two-dimensional (2D) graphene and BN are competitive candidates used as spin spintronic devices.[5-10] In analogy to graphene and BN, graphitic-C_3N_4 (g-C_3N_4) is of interest due to its promising potential applications in the field of photocatalysis.[11-13] Theoretically, carbon nitride naturally exists in different phases,[14, 15] it was believed that the graphitic structures are the most stable under ambient conditions. The widely studied g-C_3N_4 structure has two phases: the triazine-based structure and the tri-s-triazine-based structure. Experimental and theoretical studies have confirmed that the coplanar tri-s-triazine based g-C_3N_4 is more stable than triazine-based one by about 30 KJ mol^{-1}.[16-19] Recently, Zhao [20] and Lin [21] developed ultrasonic exfoliating process and mixed solvent strategy to exfoliate bulk or layered g-C_3N_4 into monolayered tri-s-triazine-based g-C_3N_4. This approach could also be used to prepare monolayered gt-C_3N_4 from its layered or bulk counterpart. Very recently, The exciting breakthrough in synthesis of gt-C_3N_4 was made by Bojdys et al. who had firstly succeeded in obtaining gt-C_3N_4 starting from dicyanamide.[22]

Though the g-C_3N_4 is non-magnetic, considerable attention has been paid to the magnetic properties of g-C_3N_4 for the spintronic applications.[23-32] To improve their performances, generally, chemical doping is an effective strategy to modify the electronic structures and magnetic properties. At the same time, the unique porous structure of g-C_3N_4 makes g-C_3N_4 a promising substrate for accommodating foreign atoms.[28-30] The 5d transition metal-doped tri-s-triazine-based g-C_3N_4 shows magnetic anisotropy, [29] and

the 3*d* transition metal-doped cases demonstrated variously structural, electronic, magnetic, and optical properties.[28, 30] Compared with the strength of spin-orbit coupling found in conventional 3*d* transition metal systems, ferromagnetic 2D materials with magnetism arising from pure *sp* electron present relatively weak spin-orbit coupling and could give a large spin relaxation time that are more suitable for future-generation spintronic devices.[27, 33] Therefore, Hydrogenation [23, 24] and doping with light elements[25-27] were adopted to induce spin related information in g-C_3N_4-based materials. It is intriguing that the carbon self-doping induces long-range ferromagnetic and anti-ferromagnetic orders deepening on the doping sites in 2D tri-s-triazine-based g-C_3N_4.[26] On the other hand, the carbon self-doping produced a ferromagnetic ground state and intrinsic half-metallicity in gt-C_3N_4.[2]

With the considerations above in mind, we have investigated the interstitial doping effect on the structure, electronic and magnetic properties of gt-C_3N_4 doped with B, Al and Cu elements. Our calculations indicated that B atoms prefer to be situated at the center of triazine ring, whereas Al and Cu atoms prefer to locate above the center of triazine ring. The doped structures are thermodynamically stable. Each dopant atom induces a local magnetic moment of 1.0 μ_B for all cases, irrespective of the doping site. Our calculations indicated that B- and Al-doped cases show half-metallic ferromagnetism that makes them more suitable for spintronic devices in future, while Cu-dped case is anti-ferromagnetic ground state.

2. Calculation details

Computational results are based on the spin density functional theory using the generalized gradient approximation (GGA) of Perdew-Burke-Ernzerhof (PBE),[34] as performed in the Vienna *ab initio* simulation package (VASP).[35, 36] The projector augmented wave method is used to describe the electron-ion interaction.[37] A kinetic energy cutoff is consistently set at 480 eV for the plane-wave expansion, which is found to be sufficient to obtain an excellent convergence to 1 meV for total energy. The conjugate gradient minimization is used for geometrical optimization until the force on each individual atom is smaller than 0.002 eV/Å. To avoid the interaction between g-C_3N_4 monolayer and its images in neighboring cells, the vacuum region between two

neighboring layers is set larger than 12 Å. The 2D Brillouin zone of gt-C_3N_4 is sampled using Gama-center Monkhorst-Pack scheme.[38] A primitive (1 × 1) g-C_3N_4 used in this study is composed of 7 atoms, 4 of which are nitrogen atoms and 3 are carbon atoms. To explore the electronic structures and magnetic properties of nonmagnetic element embedded graphitic carbon nitride sheets, we have modeled a (2 × 2) gt-C_3N_4 supercell with one nonmagnetic atom at a porous site (Fig. 1). In order to explore the magnetic ground state of gt-C_3N_4, an antiferromagnetic (AFM) configuration has been considered by using a (4 ×4) supercell. For (2 × 2) supercell, Monkhorst–Pack sampling (9 × 9 × 1) and (5 × 5 × 1) *k*-point meshes are adopted for the density of states (DOS) and the structural optimization, respectively. For (4 × 4) supercell, Monkhorst–Pack sampling (5 × 5 × 1) and (3 × 3 × 1) *k*-point meshes are adopted for the DOS and the structural optimization, respectively.

To determine whether the dopants can be positioned at the center of triangular pores, as shown in Fig. 1(a), the formation energy was calculated using the following formula.

$$E_f = E_{embedded} - E - \mu_X$$

where $E_{embedded}$ and E are the total energy of gt-C_3N_4 with and without the embedded atoms, respectively. μ_X denotes the chemical potential of the X atom and is taken as the total energy of an isolated X atom in its bulk phase.

3. Results and discussions

The geometry of gt-C_3N_4 under this study is built on triazine (C_3N_3) rings with a hexagonal unit cell. The lattice constants of gt-C_3N_4 are calculated to be 4.73 Å and 8.02 Å for planar and corrugated structure, respectively. The resulting equilibrium structure is found to spontaneously adopt a stable buckled geometry. This are consistent well with the previously reported.[22, 39] The energetic cost of "flattening" the layer is of only 0.0128 eV/atom,[39] which indicates that planar gt-C_3N_4 in principle be available by deposition on a suitable planar substrate, such as quartz glass.[40] Therefore, we take the planar structure as initiating structure. In the structure of gt-C_3N_4, there are two kinds of inequivalent N atoms: One three-coordinated N atom and three two-coordinated N atoms, as shown in Fig. 1(a). Consequently, we have considered five different types of absorption sites: above the center of the hexagonal ring of triazine (1 site), above the center of the porous of g-C_3N_4 (H site), above the carbon atom (2 site), above the three- (3 site), and

two-coordinated (4 site) N atom, respectively, as shown in Fig. 1(a). The X atoms were initially placed at the top of the five sites with a distance of 1.5 Å between the adatoms and the gt-C_3N_4 sheet. After structure optimization, it is found that adatoms always move away from (1 site) sites and have the highest total energies, while the adatoms at the top of site (4 site) always move to the top of the porous site (H site) with the lowest total energies. The total energy difference between the highest and lowest energies is about 7, 3 and 2 eV for B, Al and Cu absorptions, respectively. Therefore, the most stable site is above the center of the porous of gt-C_3N_4. To further determine whether the absorption can be achieved, the formation energies for all the possible configurations are calculated. The corresponding formation energies are about -1.10, -1.15 and 1.28 eV. The negative formation energies indicate that the absorption of B or Al atom is fairly easy.

To examine if the doped atoms will cluster together, we calculated the total energy for dopant atom diffusing along two different orientations. For Al and Cu dopants, they move parallel to *xy* plane along the two lines: H→C and H→N, as shown in the inset of Fig. 2. Here the H site is the equilibrium site for dopants and is viewed as a starting point for atomic diffusion. For B dopant, the B firstly goes along the *z* axis about 0.8 Å, and then does the same as Al or Cu do. As is shown in Fig. 2, the trapped Cu atoms should cross the minimal energy barrier of 11.2 eV in the H→N direction to cluster with another Cu atom in the neighboring H site. The minimal energy barriers are of 7.6 and 5.4 eV in the H→C direction for B and Al cases, respectively. Therefore, it is reasonable to believe that the potential wells are large enough to surmount the clustering between the doped atoms.

Fig. 1 displays atomic structures of top and side views of B-, Al-, and Cu-doped gt-C_3N_4. It can be clearly seen that absorptions result in notable buckled geometries. The buckling height, which is the distances between two farthest atom planes, is 0.528, 0.946, and 1.124 Å. Buckling causes the lone pairs on the two-coordinated nitrogen atoms to reorient and become misaligned, thus reducing their steric repulsion and stabilizing the buckled configurations.[39] It has been found that the triangular N vacant sites are the electrostatic potential valleys and the charge on N is directed away from the C-N bond toward the vacant site.[25, 27] Therefore, cations, (in particular, trivalent cations) are inclined to situated at this site and bond with the three N via valence bond. The B is seat

at the center of the triangular nitrogen hole with B-N bond of 1.425 Å which is nearly close to that of the BN (1.45 Å) phase in two dimensional honeycomb structure.[41] The corresponding bond length is about 1.79 Å (which is equal to that of the phase in two dimensional honeycomb structure.) and about 1.89 Å for Al-N and Cu-N bonds. Obviously, the size of the triangular nitrogen cavity is not larger enough to accommodate Al and Cu ions, which make them seated at the top of the triangular nitrogen cavity. Also, we further consider the situation that adatoms were initially placed at the center of triangular nitrogen cavity of gt-C_3N_4. After full geometry optimization, we found that the adatoms almost remain in the plane of the gt-C_3N_4 sheet, so that the distortion of the gt-C_3N_4 sheet is negligible. However, in comparison with the buckled geometries, the corresponding planar structures have higher energies of 0.237, 4.793 and 4.0 eV per (2 × 2) gt-C_3N_4 supercell with one B, Al and Cu atoms, respectively. After the geometrical optimization, the initially corrugated or planar gt-C3N4 structures always converge to stable buckled geometries. In the following sections, we only focus on discussing the most stable structures.

Foreign atom doped into gt-C_3N_4 system and hence injects valence electron or hole, which certainly will influence the electronic and magnetic properties of gt-C_3N_4. The difference in total energy between the spin-polarized and non-spin-polarized solutions is 61.4, 51.2, and 16.8 meV for B, Al, and Cu doped cases, respectively. The spin-polarized phase of Cu doped case is not thermodynamically stable due to the smaller spin-polarization energy than the thermal energy at room temperature (30 meV). The calculated magnetic moment is found to be 1.0 μ_B per supercell with one adatom for all the three cases. The main contribution to the total magnetic moment arises from the 2*p* orbitals of the C atoms and the three nearest neighboring N atoms adjacent to the adatom, while the magnetic moments on adatoms are almost negligible. We visualize the detailed distribution of magnetic moments of all the doped cases; we plot the spin-density isosurfaces in Fig. 1(b)-(d). It is evident that the magnetic charge density is distinctly characteristic of p_z orbtials.

To explore the origin of the magnetism, we examine the electronic structures for the B, Al, and Cu doped cases. Fig. 3 illustrates the corresponding band structures and charge densities of the states (DOS). Clearly, for the three cases, one spin channel possesses a

band gap, whereas the other spin channel shows metallic character. Significantly, the doped systems show half-metallic property. Such half-metallicity is obtained without transition metals and external stimuli, so it is worth experimentally synthesizing in future. The Fermi energy shift from valance band to conduction band because the adatoms donated electrons to the system to occupy a part of conduction band, *i.e*. anti-π orbital (π*), and therefore the magnetic moments arise mainly from the p_z orbitals, making it *n*-doped in nature. This is opposite to the hole-doped gt-C_3N_4 where the σ-bonding network is broken and hence results in partially occupied p_{x+y} orbitals, and the Fermi energy shift into valance band.[24, 26] Figure 3 shows the charge transport is dominated by the spin-down electron for B-doped case, but by the spin-up electron for Al- and Cu-doped cases. Bader analysis[42] shows that the B, Al, and Cu lost about 2.06, 1.2, and 0.66 electrons, respectively, which mainly populate the composite's conduction band. Considering back-donation of electrons from ligand to the adatoms and the partially paired *p* electrons (see Figs. 4(b) and (c)), thus these transferred electrons can be regarded as 3 electrons and 1 electron for B-doped and Al- (or Cu-) doped cases, respectively. In Fig. 3 it is obvious that a peak is situated at the middle of the band-gap for Al- and Cu-doped cases. To Further insight into the origin of the peaks, the orbital-resolved partial electron DOS is shown in Fig. 4.The peaks mainly arise from the partial paired *p* electron for Al-doped case, whereas for Cu-doped case, besides a little of *p* electron, they mainly stem from the 3*d*-orbital of Cu. Addtionally, See from the DOS in Fig. 3(f) and Fig. 4(c), Cu acts as a role of donor impurity. Different from the cases of B and Al doping, the significant peak of Cu-3*d* states indicates that there are non-bonding electrons in Cu-3*d* orbitals. Therefore, the 3*d*-orbitals are fully filled with a Cu^{+1} valence state for Cu-dope gt-C_3N_4, and hence contain a minute amount of unpaired electron [28], resulting in a slight magnetic moment on Cu site. To sum up the above arguments, two electrons filled the up-spin channel and one occupied the down-spin channel, leaving Fermi level striding it for B-doped case. For Al and Cu-doped cases, one spin unpaired electron filled the up-spin channel. Therefore, the integer magnetic moments obtained above are not surprising.

As motioned above, it is interesting to find that the hole- and electron-doping lead to difference in the spatial distribution of local magnetic moments: arising from the *p*

orbitals on the *x*-*y* plane for hole-doing,[27,43] and on the *z* orientation perpendicular to the *x*-*y* plane for electron doping.[23] For comparison, orbital-resolved electron density of states are presented in Fig . 5. It is clearly visible that the top of the valence band is given by the p_x and p_y orbitals on the C and N atoms. The bottom of the conduction band is instead formed by p_z contributions on C and N atoms and is therefore a level of π* character.[39] When holes are injected, the electrons will be extracted, thus the unpaired electron could fill in p_x and p_y orbitals. If electrons are injected, the unpaired electron will occupy on p_z orbitals. This is confirmed well by Fig. 6 where we display the orbital-resolved electron density of states for B-doped case which has been taken as an example. We found that the B-doing could greatly increase the electrical conductivity because of the formation of delocalized π-bonds. Meanwhile, the narrowed band gap is 2.1 eV in the down-spin channel, which enhances its visible light absorption, indicating that carbon B-doping might enhance the photocatalytic performance.[44]

The above obtained results are based on calculations using the (2×2) supercell, and the nonmagnetic (NM) and ferromagnetic (FM) configurations have been considered. In order to determine the magnetic ground state of the doped gt-C_3N_4 systems, we adopted large-size (4×4) supercells containing 16 primitive cells. The initial spin arrangements aligned in an "antiferromagnetic" way in the same manner as that described elsewhere.[27] To estimate the strength of exchange coupling, we calculated the energy difference between AFM and FM states. We find that the FM state is energetically more stable than the AFM state by about −266, −79 and 31 meV per supercell for the B-, Al- and Cu-doped cases, respectively. This implies that the local magnetic moments favor FM coupling at zero temperature with a total magnetic moment of 4.0 μ_B in the (4 × 4) supercell for B-, Al-doped cases. However, Cu-doped gt-C_3N_4 is antiferromagnetic in the ground state. The large ferromagnetic exchange energies make these materials quite promising candidates for realizing moderate temperature 2D ferromagnetic sheets. Based on the mean field theory and the energy difference between FM and AFM states, the Curie temperature (T_C) can be estimated by the formula $k_B T_C \gamma = 2(E_{AFM} - E_{FM})$, [45] where γ is the dimension, and k_B is Boltzmann constant. The estimated T_C is about 1200, 356 and 252 K, when the doped structures are treated as a 2D system. However, since the mean field theory often overestimated the T_C, Monte Carlo (MC) simulations using the

Ising model is view as a more accurate method to estimate the Curie temperature.[28,46,47] Consulting the results in V-, Cr-, and Fe-g-C_3N_4, we could preliminarily conclude that the B-doped g-C_3N_4 system possess ferromagnetism at room temperature. Inferring from the projected DOS relevant to the 2*p* orbitals in Fig. 2, we postulate that the FM coupling of spins to be governed by the *p*–*d* hybridization-like *p*–*p* coupling interaction, which is Similar to the magnetic coupling in C- or N-doped ZnO systems.[48, 49] The delocalized p_z electrons in π*-bonds bridges long-rang FM coupling between spins on N or C sites.

It is well known that calculations based on DFT within GGA method suffer from the spurious self-interaction error [50], whose consequence is that of overrating the spatial delocalization of *p*-orbitals and significantly underestimating the size of the band gap. Therefore, the standard DFT usually tends to predict a half-metallic ground state and long-range interaction. To correct the flaw, we use the screened hybrid functional of the Heyd–Scuseria–Ernzerhof (HSE) type to substantiate the reliability of the half-metallicity. The screening parameter μ and the mixing parameter α in HSE06 are set as the default values of 0.20 $Å^{-1}$ and 0.25, respectively.[51] For comparison, the DOS obtained from HSE06 also are presented in Fig. 3. One can see a half-metallic characteristic, meaning that the DFT-GGA is accurate enough to describe the half-metallic property. Finally, we further investigate the thermal stability of B- and Al-doped systems. Ab initio molecular dynamics simulations are performed with a Nose-Hoover thermostat at 350 K for the (4 × 4) supercell, as motioned above. After running 6000 steps with a time step of 1 fs, we find that the geometry is still kept, suggesting that the B- and Al-doped systems are stable. In fact, the B-N and AL-N binding energy are robust against the thermal fluctuation corresponding to the room temperature. In Figure 7, we show the fluctuations of temperature with time during the simulation.

4. Conclusion

We present the results obtained from Ab initio density functional theory with GGA calculations for the triazine-based g-C_3N_4 monolayer doped with nonmagnetic elements (B, Al, and Cu). The dopant prefers to be situated at the center triazine ring with slight structural distrotion, whereas Al and Cu atoms are adsorbed at above the center of triazine ring, consequently resulting in distinct nonplanar structures. However, the nonplanar

structures are thermodynamically stable. The *n*-type doping induces a total magnetic moment of 1.0 μ_B per supercell with one dopant. Magnetic moment mainly stems from the p_z orbitals, due to unpaired electron in anti-π orbitals. Combining with the formation of delocalized π-bonds, all the doped systems exhibit half-metallic features. B- and Al-doped systems possess ferromagnetic ground state, but Cu-doped case has an anti-ferromagnetic ground state. The *p-d* hybridization-like *p-p* coupling is responsible for the long-range half-metallic ferromagnetic order in B- and Al-doped systems. The estimated Curie temperature means that B- and Al-doped systems are excellent candidates for spintronics applications in future. In addition, the B doping narrows the intrinsic band-gap of pristine gt-C_3N_4, which therefore increase visible light absorption and electrical conductivity.

Acknowledgments

This work was supported by The Joint Fund of Guizhou Department of Science and Technology (Grant No. HL20147227), the Specialized Research Fund for the Doctoral Program of Kaili University (Grant BS201330), the National Natural Science Foundation of China (Grant Nos. 11074069, 61176116), the Specialized Research Fund for the Doctoral Program of Higher Education of China (Grant No. 20120161130003), Natural science research project in Guizhou province department of education（Grant KY2012061).

References:

[1] S. A.Wolf, D. D. Awschalom, R. A. Buhrman, J. M. Daughton, S. von Molnar, M. L. Roukes, A. Y. Chtchelkanova, and D. M. Treger, *Science*, 2001, **294**, 1488.

[2] Y. W. Son, M.L. Cohen, S. G. Louie, *Nature*, 2006, 444(7117), 347-349.

[3] E. J. Kan, Z. Li, J. Yang, J. G. Hou, *J. Am. Chem. Soc.*, 2008, 130(13), 4224-4225.

[4] M. S. Anwar, F. Czeschka, M. Hesselberth, M. Porcu, J. Aarts, *Phys. Rev. B: Condens. Matter Mater. Phys.*, 2010, 82(10), 100501.

[5] O. V. Yazyev, M. I. Katsnelson, *Phys. Rev. Lett.*, 2008, 100(4), 047209.

[6] D. Pesin, A. H. MacDonald, *Nat. Mater.*, 2012, 11(5), 409-416.

[7] E. J. Kan, H. J. Xiang, F. Wu, C. Tian, C. Lee, J. L. Yang, M. H. Whangbo, *Appl. Phys. Lett.*, 2010, 97(12), 122503.

[8] A. Hashmi, J. Hong, *J. Magn. Magn. Mater*, 2014, 355, 7-11.

[9] X. Li, J. Zhou, Q. Wang, Y. Kawazoe, P. Jena, *J. Phys. Chem. Lett*. 2013, 4, 259−263.

[10] X. Li, S. Zhang and Q. Wang, Phys. Chem. Chem. Phys., 2013, 15, 7142.

[11] M. Shalom, S. Gimenez, F. Schipper, I. Herraiz-Cardona, J. Bisquert, M. Antonietti, *Angew. Chem.*, 2014, 126, 3728–32.

[12] X. Li, J. Chen, X. Wang, J. Sun, M. Antonietti, *J. Am. Chem. Soc.*, 2011, 133, 8074–7.

[13] J. Oh, S. Lee, K. Zhang, J. O. Hwang, J. Han, G. Park, S. O. Kim, J. H. Park, S. Park, *Carbon*, 2014, 66, 119–25.

[14] A. Liu and M. Cohen, *Science*, 1989, 245, 841.

[15] D. M. Teter, R. J. Hemley. *Science*, 1996, 271(5245): 53-55.

[16] V. N. Khabashesku, J. L. Zimmerman, J. L. Margrave, *Chem. Mater.*, 2000, 12, 3264-3270.

[17] J. E. Lowther, *Phys. Rev. B: Condens. Matter Mater. Phys.,* 1999, 59(18), 11683.

[18] X. Ma, Y. Lv, J. Xu, Y. Liu, R. Zhang, Y. Zhu, *J. Phys. Chem. C*, 2012, 116, 23485–93.

[19] E. Kroke, M. Schwarz, E. Horath-Bordon, P. Kroll, B. Noll, A.D. Norman, *New J. Chem.*, 2002, 26, 508–12.

[20] H. Zhao, H. Yu, X. Quan, S. Chen, H. Zhao and H. Wang, *RSC Adv.*, 2014, 4, 624.

[21] Q. Lin, L. Li , S. Liang, M. Liu, J. Bi, L. Wu, *Appl. Catal. B: Environ.*, 2015, 163, 135–142.

[22] G. Algara-Siller, N. Severin, S. Y. Chong, T. Bjçrkman, R. G. Palgrave, A. Laybourn, M. Antonietti, Y. Z. Khimyak, A. V. Krasheninnikov, J. P. Rabe, U. Kaiser, A. I. Cooper, A. Thomas, M. J. Bojdys, Angew. Chem. 2014, 126, 7580 – 7585; Angew. Chem. Int. Ed. 2014, 53, 7450 – 7455.

[23] K. Xu, X. Li, P. Chen, D. Zhou, C. Wu, Y. Guo, L. Zhang, J. Zhao, X. Wu, Y. Xie, *Chem. Sci.*, 2014, 6(1), 283-287.

[24] H. Qiu, Z. Wang, X. Sheng, *Physica B: Condensed Matter*, 2013, 421, 46-49.

[25] H. Pan, H. Zhang, H. Liu, L. Chen, *Solid State Commun.*, 2015, 203, 35-40.

[26] X. Zhang, M. Zhao, A. Wang, X. Wang, A. Du, *J. Mater. Chem. C*, 2013, 1(39),

6265-6270.

[27] A. Du, S. Sanvito, S. C. Smith, *Phys. Rev. Lett.*, 2012, 108(19), 197207.

[28] D. Ghosh, G. Periyasamy, B. Pandey, S. K. Pati, *J. Mater. Chem. C*, 2014, 2(37), 7943-7951.

[29] Y. Zhang, Z. Wang, J. Cao, *J. Mater. Chem. C*, 2014, 2(41), 8817-8821.

[30] D. Ghosh, G. Periyasamy, S. K. Pati, *J. Phys. Chem. C*, 2014, 118(28), 15487-15494.

[31] A. Hashmi, J. Hong, *Sci. Rep.*, 2014, 4, 4374.

[32] D. Gao, Q. Xu, J. Zhang, Z. Yang, M. Si, Z. Yan, D. Xue, *Nanoscale*, 2014, 6(5), 2577-2581.

[33] T. Hu, A. Hashmi, J. Hong, *Sci. Rep.*, 2014, 4, 6059.

[34] J. P. Perdew, S. Burke, M. Ernzerhof, *Phys. Rev. Lett.*, 1996, 77, 3865.

[35] G. Kresse, J. Furthmuller, *Comput. Mater. Sci.*, 1996, 6, 15.

[36] G. Kresse, J. Furthmuller, *Phys. Rev. B: Condens. Matter Mater. Phys.*, 1996, 54, 11169.

[37] G. Kresse, D. Joubert, *Phys. Rev. B: Condens. Matter Mater. Phys.*, 1999, 59, 1758.

[38] H. J. Monkhorst and J. D. Pack, *Phys. Rev. B: Condens. Matter Mater. Phys.*, 1976, 13, 5188.

[39] M. Deifallah, P. F. McMillan, and F. Corà, *J. Phys. Chem. C*, 2008, 112, 5447-5453.

[40] A. I. Cooper, M. J. Bojdys, *Materials Today*, 2014, 10(17), 468-469.

[41] H. Şahin, S. Cahangirov, M. Topsakal, E. Bekaroglu, E. Akturk, R.T. Senger, S. Ciraci, *Phys. Rev. B: Condens. Matter Mater. Phys.*, 2009, 80(15), 155453.

[42] G. Henkelman, A. Arnaldsson, and H. Jónsson, *Comput. Mater. Sci.*, 2006, 36, 25.

[43] J. Zhang, X. Gong, B. Xu, Y. Xia, J. Yin, and Z. Liu, *Phys. Status Solidi B*, 2014, 251, 1386–1392.

[44] G. Dong, K. Zhao and L. Zhang, *Chem. Commun.*, 2012, 48, 6178–6180.

[45] J. Kudrnovsky, I. Turek, V. Drchal, F. Maca, J. Masek, P. Weinberger, P. Bruno, *J. Supercond.*, 2003, 16, 119.

[46] J. Zhou and Q. Sun, *J. Am. Chem. Soc.*, 2011, 133, 15113–15119.

[47] M. Kan, J. Zhou, Q. Sun, Y. Kawazoe, P. Jena, *J. Phys. Chem. Lett.*, 2013, 4, 3382−3386.

[48] H. Pan, J. B. Yi, L. Shen, R. Q. Wu, J. H. Yang, J. Y. Lin, Y. P. Feng, J. Ding, L. H. Van, J. H. Yin, *Phys. Rev. Lett.* 2007, 99, 127201.

[49] L. Shen, R. Q. Wu, H. Pan, G. W. Peng, M. Yang, Z. D. Sha, Y. P. Feng, *Phys. Rev. B: Condens. Matter Mater. Phys.*, 2008, 78, 073306.

[50] S. Lany, A. Zunger, *Phys. Rev. B: Condens. Matter Mater. Phys.*, 2008, 78, 235104.

[51] J. Heyd, G. E. Scuseria, and M. Ernzerhof, *J. Chem. Phys.*, 2006,124, 219906.

Figure captions

Figure 1. Schematic illustration of two dimensional (2 × 2) gt-C_3N_4 supercells: (a) without impurity, (b) with one B atom, (c) with one Al atom, and (d) with one Cu atom. Numbers 1–4 denote five different absorption sites, H is the center of the hexagonal ring of triazine. The blue regions represent spin electron density. Up-panel and down-panel donates top and side views, respectively.

Figure 2. The total energetics of B, Al, and Cu moving from H to C and from H to N. The diffusing paths H→C and H→N, which is divided into sections with equal lengths, are given in the inset.

Figure 3. Band structures obtained from GGA for (a) B-, (b) Al- and (c) Cu-doped gt-C_3N_4 monolayer. Total density of states obtained from GGA and HSE06 for (d) B-, (e) Al- and (f) Cu-doped gt-C_3N_4 monolayer. The red and black lines plotted in left panel refer to up- and down spin states, respectively. The dashed line indicates the Fermi energy.

Figure 4. The projected density of states for (a) B-, (b) Al-, (c) Cu- doped g-C_3N_4 monolayer. The Fermi level is set to zero energy and indicated by the vertical dashed line.

Figure 5. Orbital-decomposed DOS of pristine gt-C_3N_4 monolayer. Symbols of N_{2c} and N_{3c} denote the two-coordinated and three-coordinated nitrogen, respectively. *x*, *y*, and *z* indicate the symmetry of the atomic orbitals on which the projections are made. The vertical dashed lines represent the Fermi energy.

Figure 6. Orbital-decomposed DOS for the B-doped gt-C_3N_4. The Fermi level is plotted with dashed line.

Figure 7. Changes of temperature with time obtained from molecular dynamics simulations of B-, Al- and Cu-doped gt-C_3N_4 systems.

FIG. 1

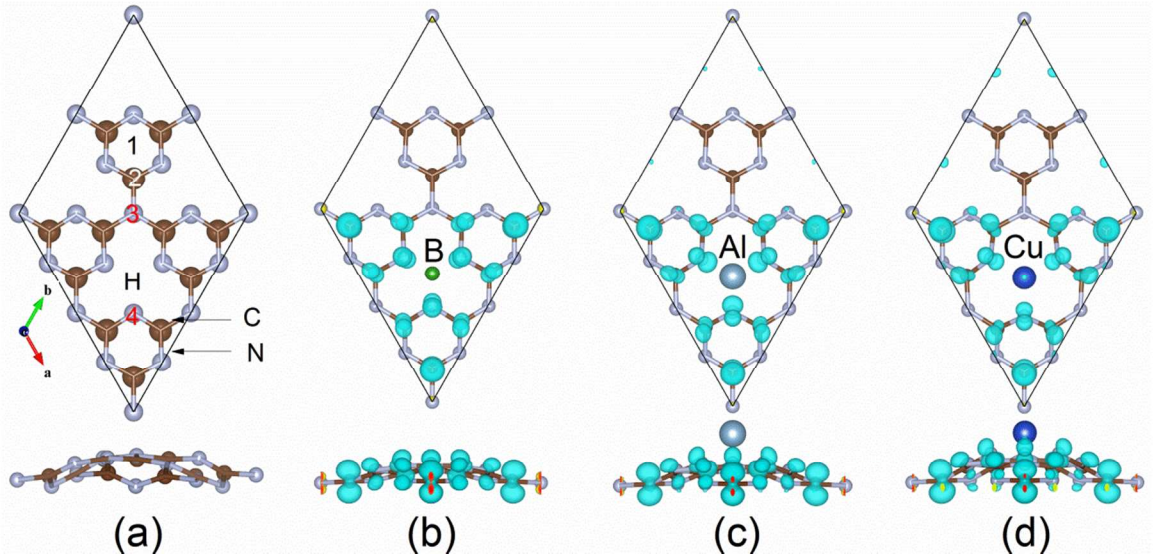

Figure 1. Schematic illustration of two dimensional (2 × 2) gt-C_3N_4 supercells: (a) without impurity, (b) with one B atom, (c) with one Al atom, and (d) with one Cu atom. Numbers 1–4 denote five different absorption sites, H is the center of the hexagonal ring of triazine. The blue regions represent spin electron density. Up-panel and down-panel donates top and side views, respectively.

FIG. 2

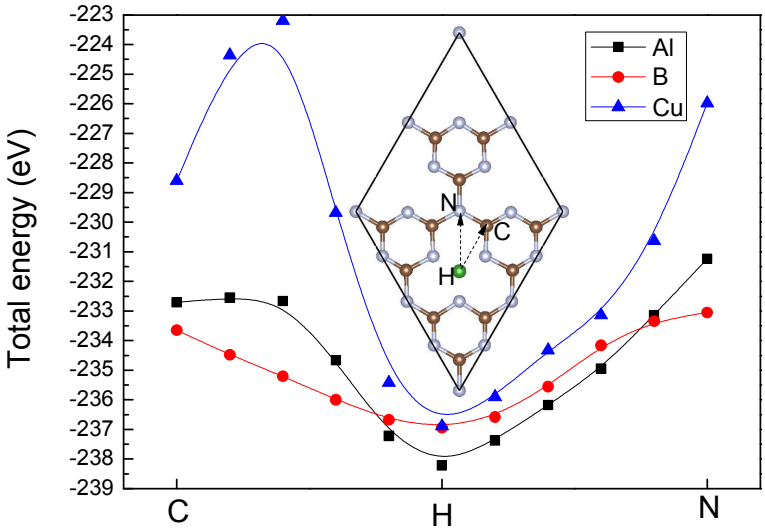

Figure 2. The total energetics of B, Al, and Cu moving from H to C and from H to N. The diffusing paths H→C and H→N, which is divided into sections with equal lengths, are given in the inset.

FIG. 3

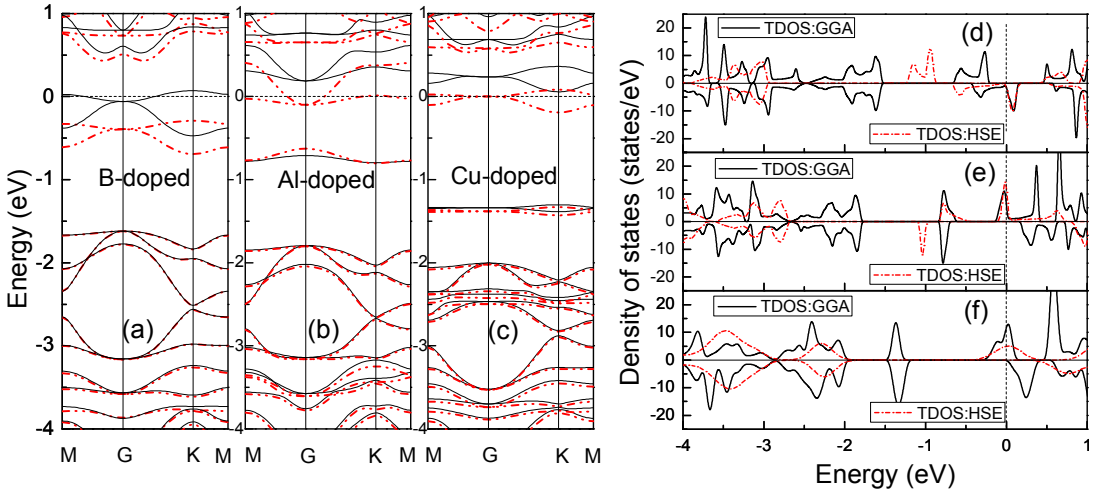

Figure 3. Band structures obtained from GGA for (a) B-, (b) Al- and (c) Cu-doped gt-C_3N_4 monolayer. Total density of states obtained from GGA and HSE06 for (d) B-, (e) Al- and (f) Cu-doped gt-C_3N_4 monolayer. The red and black lines plotted in left panel refer to up- and down spin states, respectively. The dashed line indicates the Fermi energy.

FIG. 4

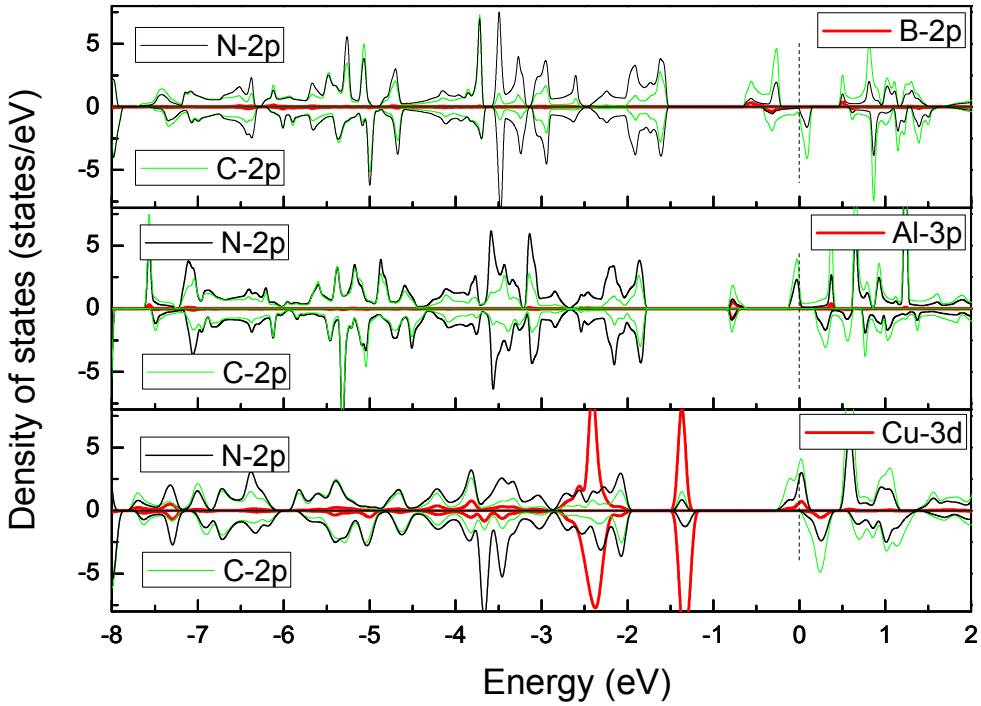

Figure 4. The projected density of states for (a) B-, (b) Al-, (c) Cu- doped g-C_3N_4 monolayer. The Fermi level is set to zero energy and indicated by the vertical dashed line.

FIG. 5

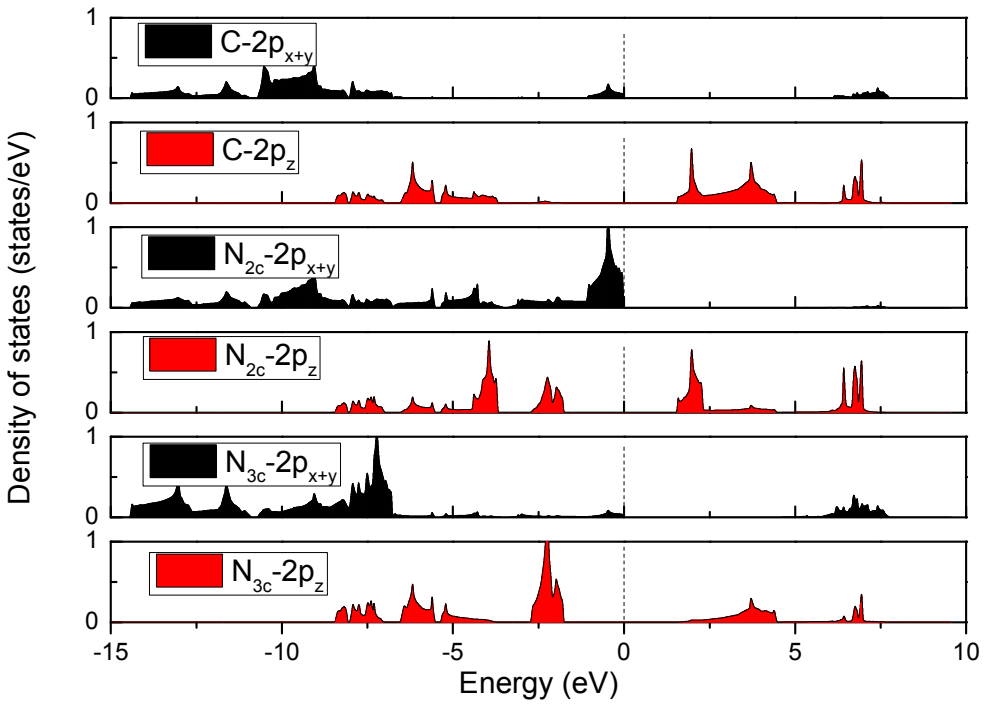

Figure 5. Orbital-decomposed DOS of pristine gt-C_3N_4 monolayer. Symbols of N_{2c} and N_{3c} denote the two-coordinated and three-coordinated nitrogen, respectively. *x*, *y*, and *z* indicate the symmetry of the atomic orbitals on which the projections are made. The vertical dashed lines represent the Fermi energy.

FIG.6

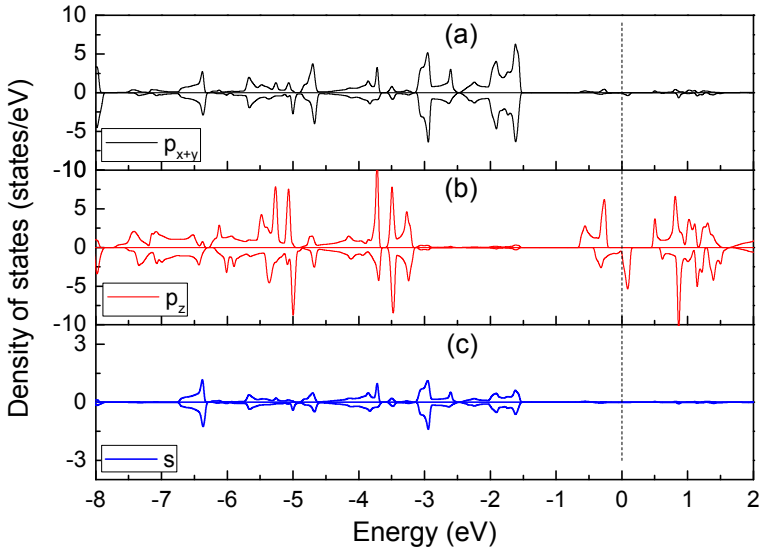

Figure 6. Orbital-decomposed DOS for the B-doped gt-C_3N_4. The Fermi level is plotted with dashed line.

FIG. 7

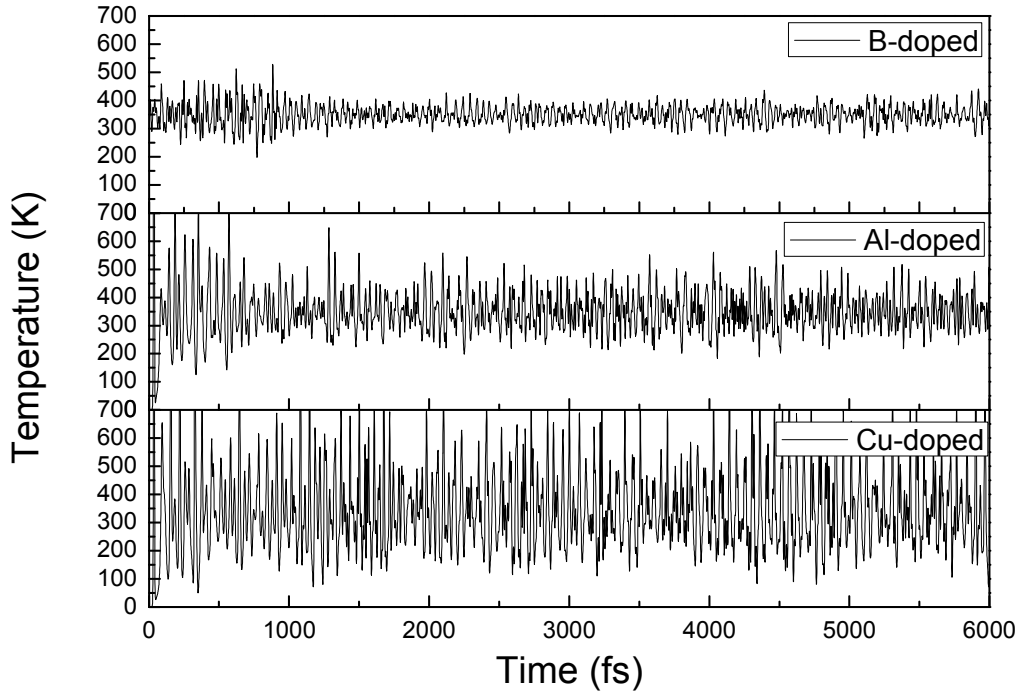

Figure 7. Changes of temperature with time obtained from molecular dynamics simulations of B-, Al- and Cu-doped gt-C_3N_4 systems.